Electric Power Systems Research 178 (2020) 106005

Contents lists available at ScienceDirect

Electric Power Systems Research

journal homepage: www.elsevier.com/locate/epsr

Dynamic characteristics of virtual inertial response provision by DFIG-based wind turbines

Matej Krpan*, Igor Kuzle

University of Zagreb, Faculty of Electrical Engineering and Computing, 10000 Zagreb, Croatia

ARTICLE INFO

Keywords:
Wind energy integration
Power system dynamics
Wind turbine dynamics
DFIG
Frequency control
Virtual inertia
Inertial response
Synthetic inertia

ABSTRACT

Power converter technology partially or fully electrically decouples the wind energy source from the grid which results in the decrease of system inertia. However, when those units participate in virtual inertial response their electromechanical dynamics become coupled to the grid electromechanical modes. To date, there were no comprehensive studies on how do different elements and parameters of a wind energy conversion system (WECS) impact its virtual inertial response provision. This is important from the standpoint of understanding the expected wind farm response during frequency containment process as well as from the standpoint of developing better inertial response controllers. In this paper we have investigated how do operating point, line-side and machine-side converter, phase-locked loop and pitch angle control impact the inertial response of the total power controlled type III WECS (DFIG) which is one of the most common wind turbine topologies used today. We show that the operating point, pitch angle control and outer loop of the machine-side converter have a visible impact on strength of the inertial response, while other elements do not and some can even be neglected in inertial response studies.

1. Introduction

A high rate of penetration of renewable energy sources (RES) in the last decade has brought along certain problems for power systems of today as well as for power systems of tomorrow. Variable and stochastic RES (of which wind energy and solar photo-voltaic (PV) energy are the most prolific representatives) are connected to the grid via power electronic interface which ensures power production at the rated grid frequency. Connection of this converter-connected generation and de-commissioning of large synchronous units has a couple of consequences:

1. grid inertia is reduced since power electronics decouple the rotating mass from grid frequency (in the case of PVs there is no rotating mass);
2. traditionally, these sources operate at the maximum power point and do not ensure a certain amount of upward reserves [1]

That is why a lot of attention has been given to developing auxiliary control algorithms for type-III and type-IV wind energy conversion systems (WECSs) which enable the utilization of their decoupled kinetic energy to respond to frequency disturbances, usually named *virtual or synthetic inertia* [1–8]. Moreover, WECSs can be operated according to some sub-optimal power curve which ensures a certain amount of power reserve during normal operation [9–13,6,14]. Then, droop control can be added to enable the participation of wind turbine generators (WTGs) in primary frequency control (PFC). This is a heavily researched topic on which we will spend no more time on and we refer the reader to [15] to read more about frequency support services from WPPs. Nevertheless, WECSs are complex electromechanical systems and there were no comprehensive studies on how exactly do different parameters and the operating point impact the inertial response and droop control capabilities of a type-III or type-IV WECS. Type-III wind turbines are usually called doubly-fed induction generator (DFIG) wind turbines and we will use this term onward.

1.1. Literature survey

Kayikçy and Milanović [16] thoroughly investigated the impact of model order of a DFIG-based wind turbine on transient response (short-circuit) and they concluded the following: constant wind power or constant mechanical torque assumptions are not realistic; simplification

* Corresponding author.
E-mail addresses: matej.krpan@fer.hr (M. Krpan), igor.kuzle@fer.hr (I. Kuzle).

[1] today, most grid codes require that wind power plants have the capability of an upward reserve, but most of them do not require wind farms to continuously operate with that reserve

https://doi.org/10.1016/j.epsr.2019.106005
Received 9 April 2019; Received in revised form 22 July 2019; Accepted 13 August 2019
Available online 17 September 2019

Nomenclature

*	Superscript denoting a set-point value (reference)
$_d$	Subscript denoting d-axis value
$_q$	Subscript denoting q-axis value
β	Pitch angle
γ	Shaft twist angle
λ	Tip-speed ratio
ρ	Air density
ω_g	Electric angular frequency of the generator rotor
ω_s	Electric angular frequency of the grid ($\omega_s = 2\pi f_s$)
ω_t	Mechanical angular frequency of the turbine
$C_p(\lambda, \beta)$	Wind turbine power coefficient
D_s	Shaft damping constant
H_g	DFIG inertia constant
H_t	Wind turbine inertia constant
K_p	Proportional gain of a PI controller
K_i	Integral gain of a PI controller
K_s	Shaft stiffness
K_v	Virtual inertia constant
R	Wind turbine rotor radius
T_g	Generator electrical torque
T_m	Turbine mechanical torque
T_s	Pitch servo time constant
v_w	Wind speed
DFIG	Doubly fed induction generator
PLL	Phase-locked loop
MSC	Machine-side converter (rotor-side converter)
LSC	Line-side converter (grid-side converter)
MPPT	Maximum power-point tracking
PWM	Pulse-width modulation
SG	Synchronous generator
RMS	Root mean square
VIR	Virtual inertial response
ROCOF	Rate-of-change-of-frequency
WECS	Wind energy conversion system
WTG	Wind turbine generator

of the converter and machine models does not significantly influence the transient response of the DFIG; DC voltage can be assumed constant. In [17], the same authors analyzed the impacts of the following aspects on system frequency response: control strategy (power or torque), maximum-power-point-tracking (MPPT) characteristic, initial loading and auxiliary inertial controller parameters. They concluded that torque control is more stable than power control, MPPT curve provides a self-stabilizing mechanism, initial loading has a significant impact of inertial response provision due to the converter limits and that various power and frequency responses could be obtained depending on the design of the inertial controller, but no sensitivity analysis was done. In some of our recent work [18,19], we have analyzed the small-signal response of a total power controlled variable speed wind turbine (VSWT) and we have shown the following: impact of the operating point on the combined VIR and PFC depends on the control structure, more precisely on the power tracking and set-point curve. Weaker response is generally recorded for higher wind speeds. However, the design of the deloaded curve around the maximum rotor speed results in a stronger and more oscillatory response which can sometimes be unstable. We have also shown that the inertia of the wind turbine doesn't have a significant impact on the grid frequency following a disturbance except in the aforementioned region where bigger wind turbines result in deteriorated frequency response. The former is in line with the well-known decoupling effect of power converters, while the latter is a consequence of the power set-point algorithm. Pitch angle servomechanism time constant doesn't have an effect at above rated wind speeds, while in the region around maximum rotor speed slower pitch angle control results in a more oscillatory behaviour of the grid frequency. However, in [18,19], simplified wind turbine model was used (generator and electrical control were not taken into account). The grid was replaced by a simple low-order system frequency response model with turbine dynamics. Recently, research has shown [20,21] that there is a link between the virtual inertial response (VIR) and phase-locked loop (PLL) which can affect both the small-signal stability of the power system and the strength of the VIR. Arani and Mohamed [22] analyzed the impacts of *droop* control in DFIGs on microgrid and weak grid stability and they also concluded that torque control is more stable than power control. They have also shown that pitch angle controller does not have a significant impact on droop control, but no studies on inertial response were done. Quan and Pan [23] analyzed the impact of operating point of a total power controlled DFIG on simultaneous provision of inertial response and droop response using the model linearization and they have concluded the following: power injection is stronger under lower wind speeds in the medium wind speed region (where power is proportional to the cube of the generator speed). They did not analyze behaviour under low wind speeds nor under high wind speeds. On the other hand, Hu et al. [24] showed that the inertial response of a torque-controlled DFIG is stronger under higher wind speeds (in the MPPT region). They also showed that the higher PI gains of the speed controller weaken the inertial response due to the bigger restraining effect. However, they used a simplified DFIG model. Based on the literature survey, a comprehensive study is

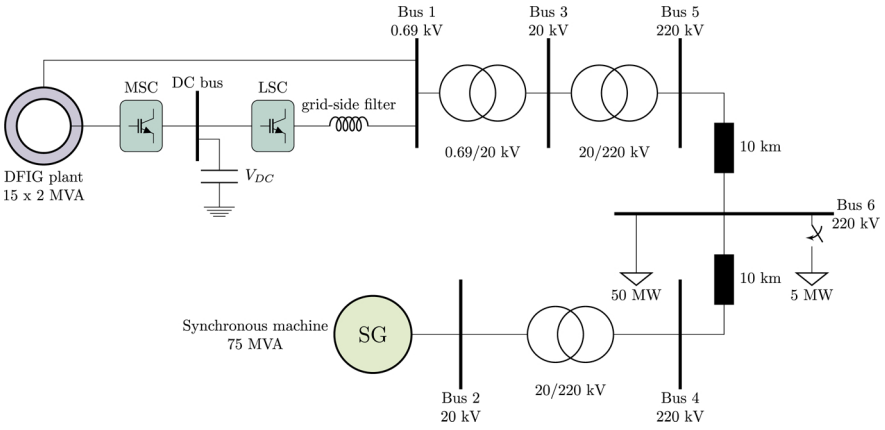

Fig. 1. Test system.

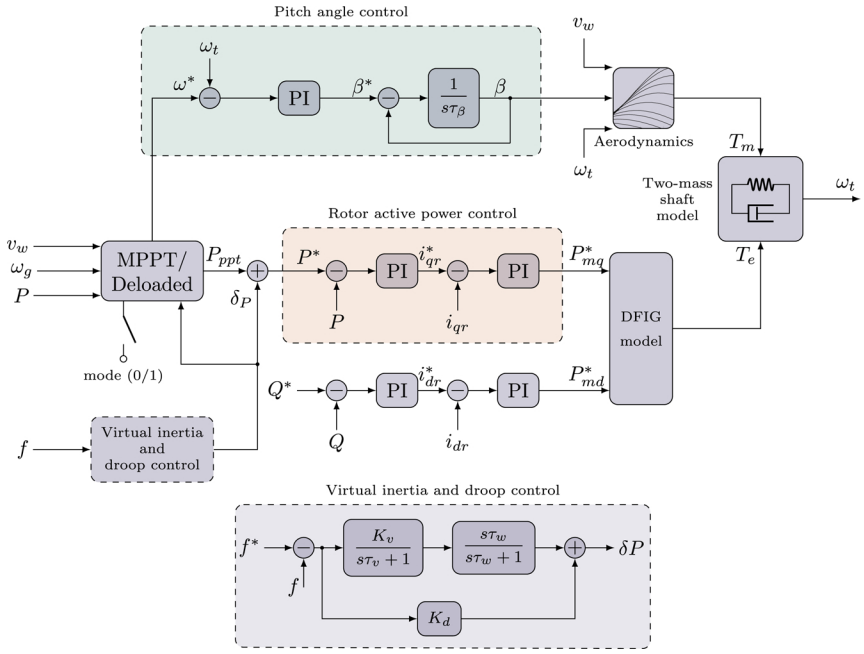

Fig. 2. wind turbine model and control system.

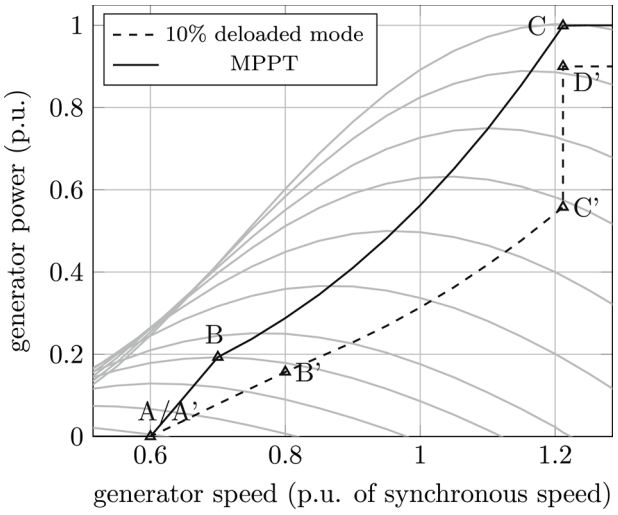

Fig. 3. Power vs. generator speed curve of the test DFIG.

required to analyze the impact of various parameters on virtual inertial response from DFIGs. With that being said, this paper is based upon preliminary analysis from [25] and it contains much more exhaustive analysis.

1.2. Contribution

Based on the literature survey, one can see that there were no comprehensive studies on the sensitivity analysis of various DFIG elements on inertial response provision. These elements are: machine-side converter (MSC) and line-side converter (LSC) controller parameters, PLL parameters, pitch angle controller parameters and initial operating point). The active power response of a DFIG-based wind turbine and the impact of the aforementioned parameters heavily depend on the type of the control design of the WECS. Furthermore, no multidimensional analysis was done in any of the surveyed literature from Section 1.1. In this paper, we have focused on the total power control as one of the frequently used schemes in the literature. The main contribution of this paper is to understand how different elements of a DFIG WECS impact the provision of inertial response in order to facilitate further research regarding wind turbine control design as well as to shed light onto the fact that different responses from wind farms may be expected during frequency containment process. To the best of our knowledge, this is something that was not done before. Furthermore, we note that the response of the WECS to frequency disturbance differs between different types of models in some aspects. This is an important finding because using different models can result in arriving to contradictory conclusions while doing power systems research.

Therefore, the contributions of this paper are as follows:

- analysis of the impact of the DFIG operating point on VIR for the whole operating regions from cut-in to cut-out;
- multidimensional sensitivity analysis of the impact of the DFIG control system parameters on the dynamic characteristics of the VIR;
- to clarify, illustrate and discuss in detail the characteristics of the total power control of DFIG WECS and how it affects the provision of virtual inertia;
- finding that inertial response sensitivity to initial conditions depends on the type of MPPT control algorithm.

The rest of the paper is organized as follows: In Section 2, the test system used for simulations and methodology are presented. In Section 3, we analyze and discuss the impact of the aforementioned variables on the VIR provision by the total power controlled DFIG WECS. Section 4 concludes the paper.

2. Methodology

Fig. 1 shows the test system used in the simulations. It is a two-machine system consisting of a DFIG-based wind power plant (consisting of 15 aggregated 2 MVA turbines) and a 75 MVA synchronous generator interconnected through a series of lines and transformers. Wind power penetration is equal to 28.5% of total installed capacity. Loads are connected to bus 6. We understand that this is not the most realistic depiction of a power system, but it is the simplest form of a system for studying frequency dynamics. The synchronous machine represents the rest of the bulk power system while isolating the average frequency dynamics from other factors such as grid topology,

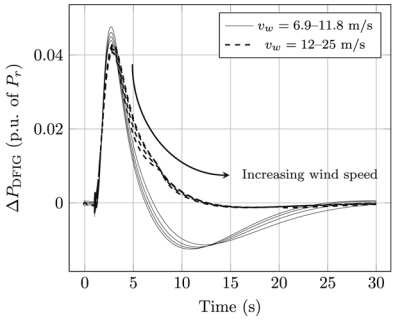

(a) DFIG power injection relative to the rated power P_r

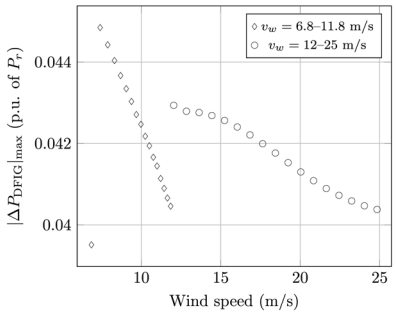

(b) DFIG power injection peak value with respect to the wind speed

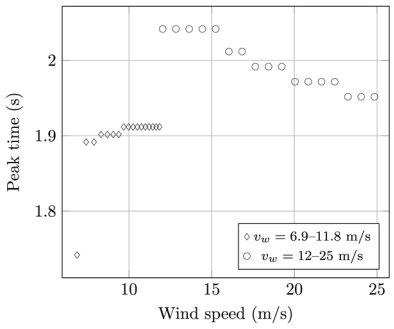

(c) DFIG power injection peak time with respect to the wind speed

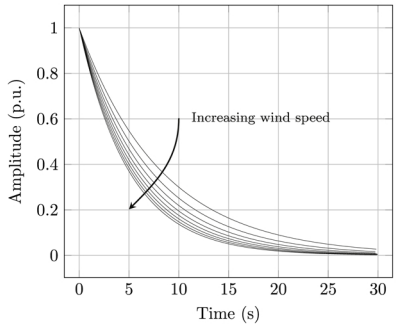

(d) Gain of the simplified wind turbine transfer function for varying initial wind speed

Fig. 4. Dynamic characteristics of the DFIG inertial response for varying wind speeds.

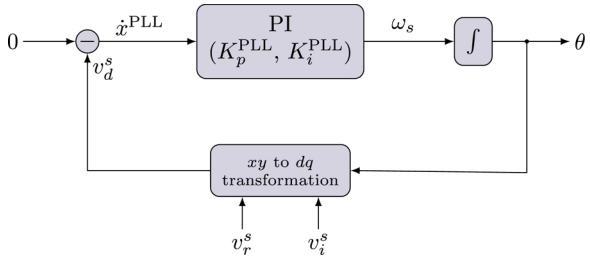

Fig. 5. Phase-locked loop model.

interaction between different controllers, different turbine types, etc. which are beyond the scope of this paper. The classical model of the synchronous machine is used and it is equipped with a *TGOV1* turbine-governor model and a *IEEET1* automatic voltage regulator (AVR). In all test cases, a frequency disturbance is induced by connecting the 5 MW load at $t = 1$ s which is equal to 5% of the total generation capacity and 10% of pre-disturbance load. Parameters of the test system are given in the Appendix. Electromechanical transient simulation (RMS values) is conducted in *DIgSILENT PowerFactory 2019* software package.

Fig. 2 shows the overall control system of the DFIG model used in this paper. MPPT or deloaded operation is set by setting the `mode` flag to 0 or 1, respectively. Fig. 3 shows the generator power vs. rotor speed curve for both MPPT and deloaded operation. However, since we are focusing on VIR, the DFIG will be operating according to the MPPT curve. Parameters of the complete wind turbine system are given in the Appendix.

Now, we briefly present the mathematical model of the DFIG wind turbine used in this paper. Wind turbine mechanical power is calculated as (1) [26]:

$$P_m(\omega_t, \beta, v_w) = \frac{1}{2}\rho R^2 \pi C_p(\omega_t, \beta, v_w) v_w^3(t), \tag{1}$$

where the aerodynamic power coefficient C_p is a complex analytic expression and can be found in [27]. Electrical power set-point P_{ppt} (power-point tracking) depends on the operating region of the turbine (Fig. 3) and is described by (2)–(4):

$$P_{\mathrm{ppt}}^{A-B/A'-B'} = \frac{P^{B/B'} - P^{A/A'}}{\omega_g^{B/B'} - \omega_g^{A/A'}} \cdot \omega_g(t). \tag{2}$$

In the region $B - C/B' - C'$ generator power is proportional to the cube of the generator speed and a coefficient k_g which can be calculated using an iterative method due to the nonlinearity of the aerodynamics [28]:

$$P_{\mathrm{ppt}}^{B-C/B'-C'} = k_g \omega_g^3(t). \tag{3}$$

In the region $C' - D'$ in deloaded mode, the maximum speed is reached and the power set-point is obtained from the estimated wind speed [29,30]:

$$P_{\mathrm{ppt}}^{C'-D'} = f(v_w)|_{\omega_g = \mathrm{const.}}. \tag{4}$$

Generator power and speed at points *ABCD/A′B′C′D′* are constant coefficients calculated during the turbine design. At points C and D' power set-point is equal to the nominal and maximum deloaded power, respectively—and the pitch angle controller restricts the turbine speed to the maximum speed. Shaft dynamics are described by the two-mass model (5):

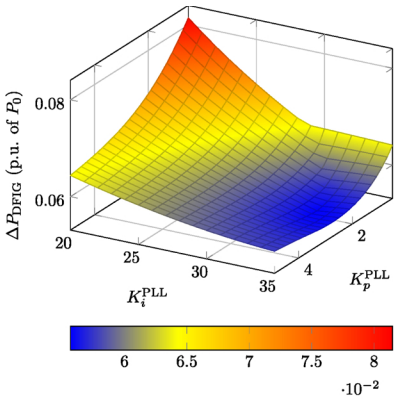

(a) DFIG power injection peak value as a function of K_p^{PLL} and K_i^{PLL} for a below rated wind speed

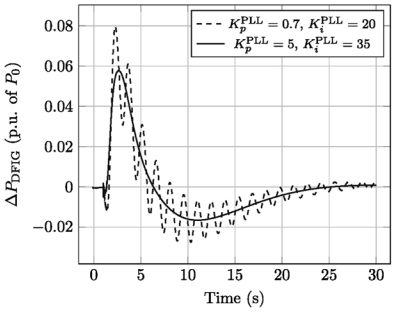

(b) DFIG power injection relative to the initial power P_0 for some characteristic combinations of K_p^{PLL} and K_i^{PLL} for a below rated wind speed

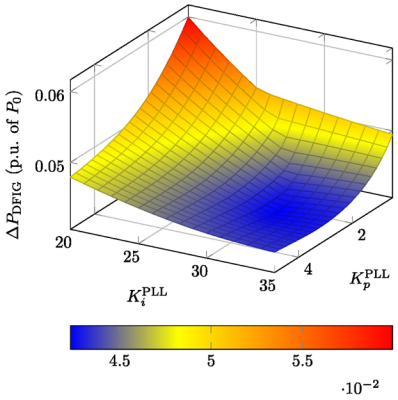

(c) DFIG power injection peak value as a function of K_p^{PLL} and K_i^{PLL} for an above rated wind speed

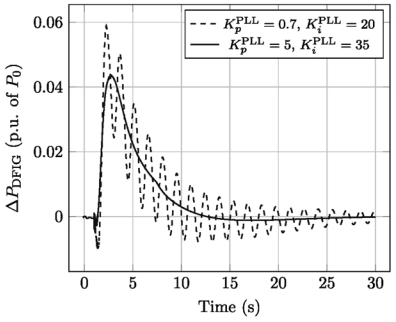

(d) DFIG power injection relative to the initial power P_0 for some characteristic combinations of K_p^{PLL} and K_i^{PLL} for an above rated wind speed

Fig. 6. Dynamic characteristics of the DFIG inertial response for different PLL PI controller parameters.

$$\begin{aligned} 2H_t \frac{d\omega_t}{\mathrm{dt}} &= T_m - K_s\gamma - D_s(\omega_t - \omega_g) \\ 2H_g \frac{d\omega_g}{\mathrm{dt}} &= K_s\gamma + D_s(\omega_t - \omega_g) - T_g \\ \frac{d\gamma}{\mathrm{dt}} &= 2\pi f_n(\omega_t - \omega_g). \end{aligned} \tag{5}$$

DFIG model is an existing element in DIgSILENT PowerFactory software modelled in rotor reference frame. It is controlled with the modulation factors P_{mq}^* and P_{md}^* from the MSC. P_{mq}^* and P_{md}^* are expressed in the rotor reference frame, however they are initially obtained in the stator-flux reference frame in which the MSC operates.

LSC as well as the DC capacitor are additionally considered as well. LSC operates in the stator-voltage reference frame. Both MSC and LSC are modelled with the fundamental frequency model (for RMS studies) of the voltage source converter element with sinusiodal PWM. The converter AC voltage V_{ac} is related to the converter DC voltage V_{dc} by (6):

$$V_{\text{ac}} = \frac{\sqrt{3}}{2\sqrt{2}} V_{\text{dc}}(P_{\text{mr}}^* + \mathrm{j}P_{\text{mi}}^*), \tag{6}$$

where P_{mr}^* and P_{mr}^* are real and imaginary parts of the modulation index depending on the reference frame used. All the MSC and LSC PI controllers are non-windup to prevent the windup effect of the integral controller.

Pitch control is described by (7). Pitch controller is also a non-windup controller. Pitch angle β is limited between 0 and 27° and the pitch rate is limited to ± 10°/s.

$$\begin{aligned} \beta^* &= K_p(\omega_t - \omega^*) + K_i \int (\omega_t - \omega^*)(\tau)d\tau \\ T_s \frac{d\beta}{\mathrm{dt}} &= \beta^* - \beta. \end{aligned} \tag{7}$$

3. Dynamic characteristics of virtual inertial response

3.1. Impact of initial wind speed

The DFIG is initialized at point B (Fig. 3) and the wind speed is linearly increased from ~7 m/s to ~25 m/s. Pitch control becomes active around 12 m/s. Inertial response is not considered in zone *AB* because of the low speed and the increased possibility of stalling. Impact of the initial conditions (initial wind speed) is visible in Fig. 4a–d. Generally, when the inertial response is activated at point *B* (in this case

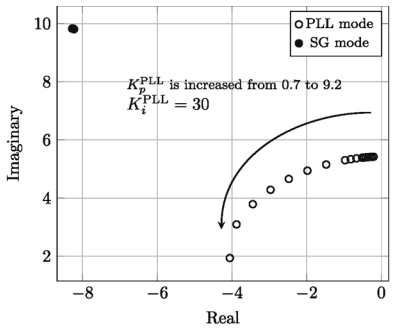

(a) Eigenvalues of the PLL and SG mode for varying K_p^{PLL}

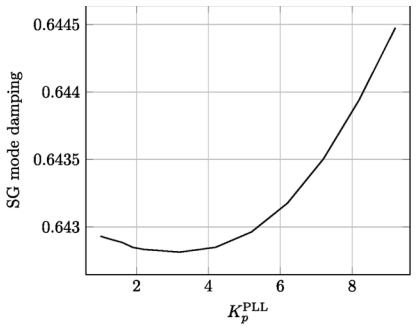

(b) Damping of the SG mode for varying K_p^{PLL}

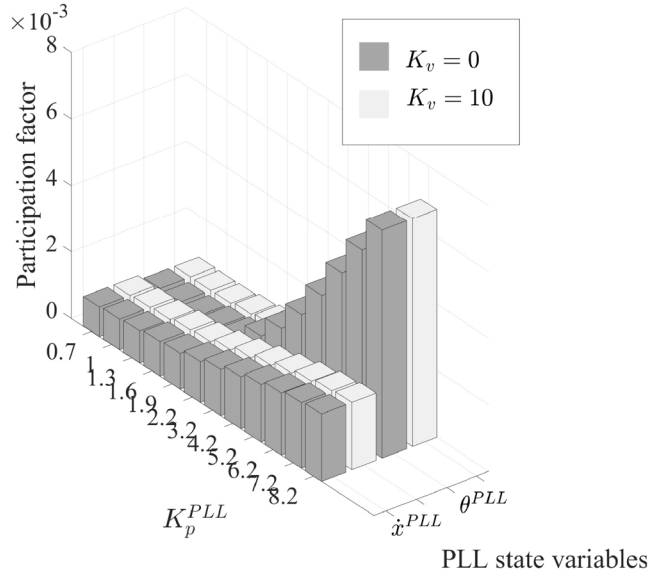

(c) Participation factors of PLL state variables in SG mode for varying K_p^{PLL} and K_v

Fig. 7. Modal analysis of the relevant system modes for different PLL PI controller parameters.

around 6.9 m/s), the generator speed will drop resulting in shifting the power set-point curve from *BC* to the line *AB*. This in turn results in slightly lower peak time, lower peak value and a larger undershoot of the power injection.

When the wind speed is high enough, the generator speed will stay in the *BC* region. Here, the peak value of the inertial response falls linearly with the wind speed while there is no significant impact on the time when the peak value is reached. The explanation can be found in the small-signal stability model of the simplified one-mass wind turbine system which has been derived in [18,23]; transfer function $G(s)$ which relates the power set-point P^* to the virtual inertia power output δP is (8) [18,19]:

$$G(s) = \frac{\Delta P^*}{\delta P} = \frac{2\mathrm{Hs} - (k_g\omega_0 + \frac{\partial T_m}{\partial \omega_g}|_0)}{2\mathrm{Hs} + 2k_g\omega_o - \frac{\partial T_m}{\partial \omega_g}|_0}. \tag{8}$$

The gain of this transfer function falls with the increasing initial generator speed (i.e. wind speed) which has been illustrated in Fig. 4d.

Once the pitch control becomes active and the power reference and generator speed are controlled to be constant, there is a step increase in the peak value compared to the previous wind speed step when pitch control was inactive. Then, the peak value of the inertial response falls non-linearly with the respect to the increasing wind speed reflecting the nonlinear nature of the pitch angle in the aerodynamic model. Slower pitch control action is reflected in the peak time compared to when only rotor speed control is utilized: peak time jumps from 1.9 s to around 2.05 s and falls of with increasing wind speed. This falloff can be attributed to the high nonlinearity of the aerodynamic part and the shortcomings of the analytical C_p curve at higher wind speeds [16]. The peak value of the inertial response can vary between 0.045 p.u. and 0.040 p.u. depending on the wind speed.

On the other hand, Hu et al. [24] used speed-controlled DFIG model with inverse MPPT characteristic (rotor controller controls the speed rather than power) and they report stronger inertial response at higher wind speed which brings us to the first conclusion: inertial response sensitivity is not the same for total power controlled DFIG and for the speed-controlled DFIG. Value of the virtual inertia constant should be dynamically changed as the function of the generator speed in order to achieve better inertial response and to achieve a consistent power injection with respect to both the pre-disturbance power output and the rated power.

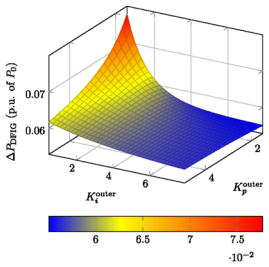

(a) DFIG power injection peak value as a function of K_p^{outer} and K_i^{outer} for a below rated wind speed

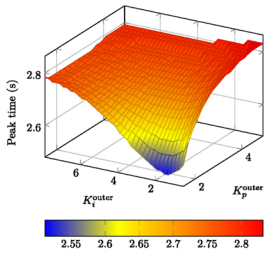

(b) DFIG power injection peak time value as a function of K_p^{outer} and K_i^{outer} for a below rated wind speed

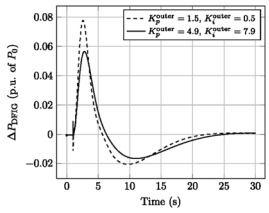

(c) DFIG power injection relative to the initial power P_0 for some characteristic combinations of K_p^{outer} and K_i^{outer} for a below rated wind speed

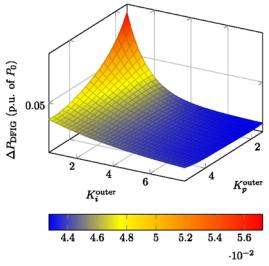

(d) DFIG power injection peak value as a function of K_p^{outer} and K_i^{outer} for an above rated wind speed

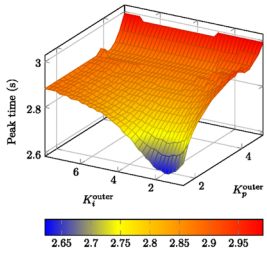

(e) DFIG power injection peak time value as a function of K_p^{outer} and K_i^{outer} for an above rated wind speed

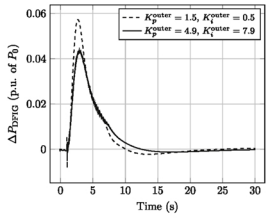

(f) DFIG power injection relative to the initial power P_0 for some characteristic combinations of K_p^{outer} and K_i^{outer} for an above rated wind speed

Fig. 8. Dynamic characteristics of the DFIG inertial response for different MSC outer PI controller parameters.

3.2. Impact of PLL parameters

Frequency signal which is used as an input to the virtual inertia controller is estimated using a PLL (Fig. 5) which measures the stator voltage at Bus 1. In the stator flux reference frame, the d-axis coincides with the stator flux vector and the q-axis coincides with stator voltage vector, and it is 90° ahead of the d-axis. The PLL controls the angle θ such that the d-axis component of the stator voltage is zeroed. In this case, θ is the angle of the stator voltage vector relative to the voltage angle at the reference bus (0°). Inputs to the PLL are the real and imaginary components of the stator voltage in the global (positive-sequence, xy) reference frame. Estimated grid frequency is equal to $f_s = \omega_s/2\pi$. The PLL model is described with (9):

$$\begin{aligned} f_s &= \frac{-1}{2\pi}\left(K_p^{\text{PLL}} v_d^s(t) + K_i^{\text{PLL}} \int v_d^s(\tau)d\tau\right) \\ \theta &= 2\pi \int f_s(\tau)d\tau. \end{aligned} \tag{9}$$

We vary K_p^{PLL} and K_i^{PLL} linearly between 1 and 35, and 20 and 35, respectively. Fig. 6 shows the dynamic characteristics of the inertial response for different PI parameters for a below rated and an above rated wind speed. The simulations have shown a few things: firstly, if K_p^{PLL} and K_i^{PLL} are large enough, they do not have a significant impact on the strength of the inertial response (Fig. 6a and c). However, for certain combinations of K_p^{PLL} and K_i^{PLL} where one or both of those gains are small, the peak is significantly higher (Fig. 6b and d) than it is for larger gains, but the complete behaviour is more oscillatory and undesirable. Smaller PI gains resulted in worse tracking and stronger oscillations.

Secondly, For smaller PI gains, the DFIG model exhibits a behaviour similar to a non-minimal phase shift system which is visible through the initial undershoot in Fig. 6b and d: in the initial moments following a disturbance, the DFIG output power is momentarily reduced further aggravating the grid frequency dynamics which in turn results in a stronger response. Worse stator voltage angle tracking will indirectly influence the DFIG dynamics because this angle is used for transforming between rotor reference frame and stator flux reference frame in the rotor-side control system. Furthermore, with smaller PI gains the damped frequency of the PLL mode is close to that of the electromechanical modes of the system which means that the PLL with participate in the electromechanical oscillations of the system. However, PLL gains are typically large and the PLL mode is well damped [31].

To the contrary, Ma et al. [20] report weaker inertial response under smaller PLL PI gains and well-damped behaviour. In their paper, they have investigated the impact of PLL dynamics on inter-area oscillations between two systems connected with a weak tie-line. We did not notice any such behaviour in our test system, even with increasing both line lengths from 10 km to 110 km. There can be multiple reasons for this discrepancy between the two results: grid topology, types of excitation systems and power system stabilizers, controllers parameters, wind turbine generator model, etc. This is a complex issue which needs

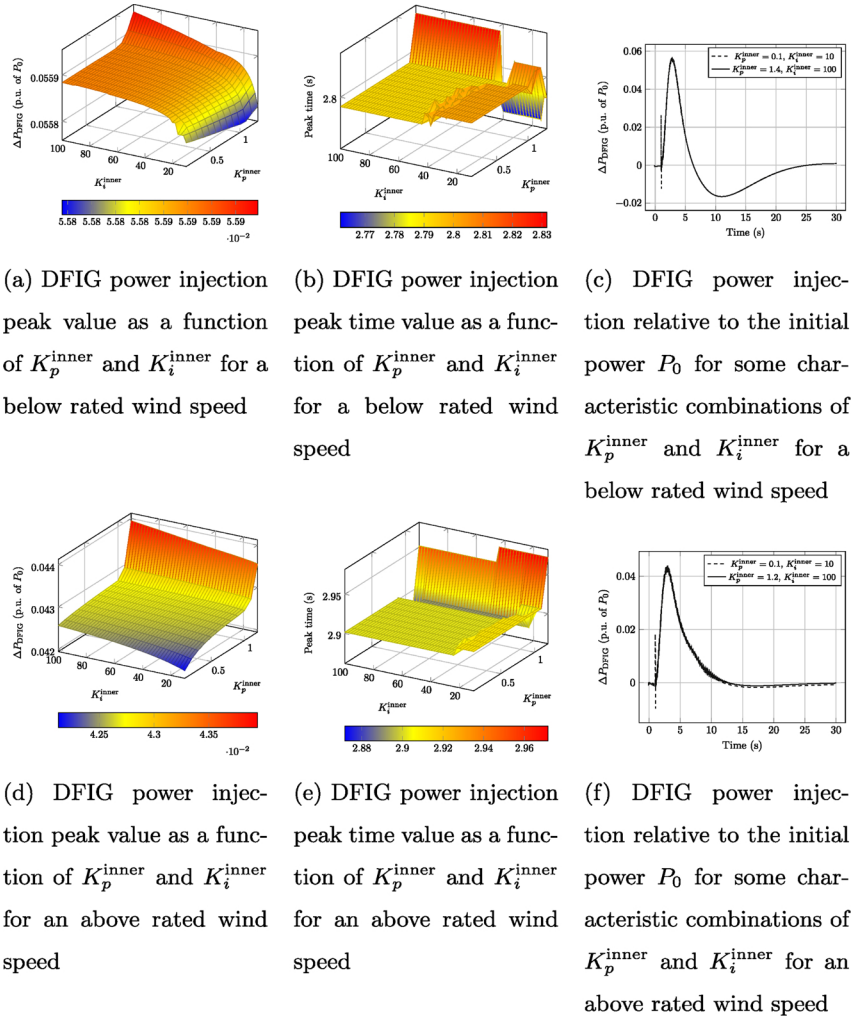

(a) DFIG power injection peak value as a function of K_p^{inner} and K_i^{inner} for a below rated wind speed

(b) DFIG power injection peak time value as a function of K_p^{inner} and K_i^{inner} for a below rated wind speed

(c) DFIG power injection relative to the initial power P_0 for some characteristic combinations of K_p^{inner} and K_i^{inner} for a below rated wind speed

(d) DFIG power injection peak value as a function of K_p^{inner} and K_i^{inner} for an above rated wind speed

(e) DFIG power injection peak time value as a function of K_p^{inner} and K_i^{inner} for an above rated wind speed

(f) DFIG power injection relative to the initial power P_0 for some characteristic combinations of K_p^{inner} and K_i^{inner} for an above rated wind speed

Fig. 9. Dynamic characteristics of the DFIG inertial response for different MSC inner PI controller parameters.

separate and in depth studies which are beyond the scope of this paper.

This behaviour is independent of whether or not the virtual inertial response is active or not and it mostly depends on the PLL itself. The participation of PLL in electromechanical oscillations is visible by plotting the trajectories of the PLL mode and the system electromechanical mode (Fig. 7). PLL mode is related to the PLL state variables $\dot{x}^{\text{PLL}}$ and $\dot{\theta}$. Synchronous generator (SG) mode has a frequency of around 1.5 Hz and can be considered a local mode. Fig. 7a shows that the parameters of the PLL PI controller do not have a significant impact on the SG mode. On the other hand, PLL mode is close to the imaginary axis for small K_p^{PLL} values (weak damping) and this oscillatory behaviour will dominate the response as seen from Fig. 6b and d. By increasing the proportional gain of the PLL, damping of this mode is increased and at certain point PLL mode ceases to be oscillatory (it is completely damped). Fig. 7c shows that the participation factor of PLL state variables in the SG mode increases for larger K_p^{PLL} gain, but does not depend on the virtual inertia coefficient.

3.3. Impact of MSC control loops

Machine side converter control system usually consists of a slower outer loop which generates the q and d axis rotor current references and a faster inner loop which generates the q and d axis rotor voltage references or similar PWM control signals (in this case, they are q and d axis modulation factors which is one possible option in DIgSILENT PowerFactory). MSC is operated in a stator-flux reference frame where q axis corresponds to the active power control and d axis corresponds to the reactive power control. Since the reactive power control is not a topic of this research, only the q axis parameters will be studied.

We mentioned that the outer loop is slower and the inner loop is faster. Parameter tuning of a PID controller is not a straightforward process and depends on the desired performance as well as on the model of the system and the type of control (power, torque or speed control [32,24,20]). Nevertheless, Hansen et al. report that better performance can be achieved with stronger integral gain. Therefore, we will approach the analysis of the impact of MSC control loops parameters on virtual inertial response by considering both weaker and stronger PI action.

3.3.1. Outer loop

K_p^{outer} and K_i^{outer} are linearly varied between 1.5 and 5, and 0.5 and 8, respectively. Fig. 8 shows the impact of MSC outer PI controller on the strength of the inertial response. For smaller PI gains the virtual inertial response is stronger (higher apex) for both below rated and above rated wind speed (Fig. 8a and d). This is because the stronger action of the outer PI loop restrains the change of the generator power more [24]. This in turn results in weaker power injection from DFIG. However, if the outer control loop is fast enough (large PI gains) than there is no impact on the strength of the inertial response as shown by the blue shaded areas in Fig. 8a and d. Furthermore, weaker PI gains will also results in faster peak time as shown in Fig. 8b and e. In time domain, this is illustrated with two responses for some characteristic strong and weak combinations of PI gains (Fig. 8c and f). In summary, this means that the dynamics of the slower outer loop should be taken

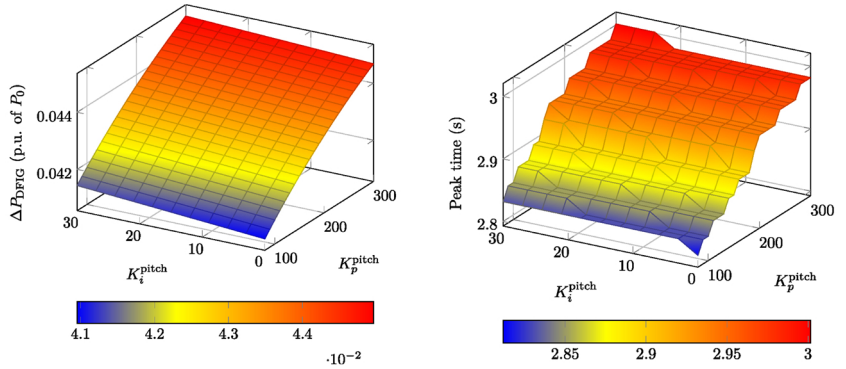

(a) DFIG power injection peak value as a function of K_p^{pitch} and K_i^{pitch}

(b) DFIG power injection peak time value as a function of K_p^{pitch} and K_i^{pitch}

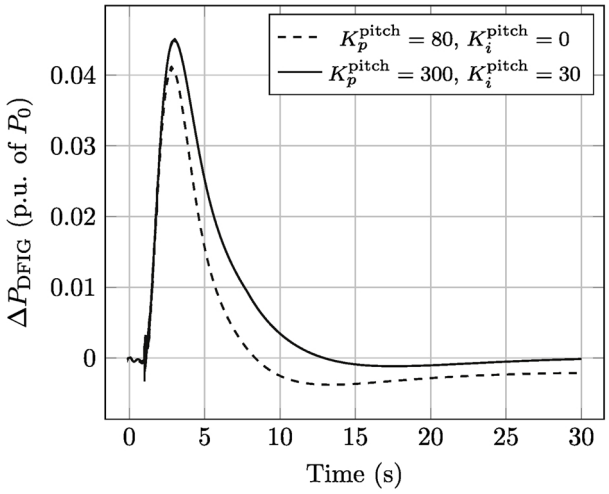

(c) DFIG power injection relative to the initial power P_0 for some characteristic combinations of K_p^{pitch} and K_i^{pitch}

Fig. 10. Dynamic characteristics of the DFIG inertial response for different pitch PI controller parameters.

into account when studying inertial response dynamics. They can only be neglected if the PI gains are large such that the whole loop has faster set-point tracking.

3.3.2. Inner loop

K_p^{inner} and K_i^{inner} are linearly varied between 0.1 and 1.4, and 10 and 100, respectively. Impact of the much faster inner loop dynamics is negligible as shown in Fig. 9. Impact on the strength of the inertial response is in the order of 10^{-4} (Fig. 9a) and the impact on the peak time is in the order of 10^{-2} (Fig. 9b). Inertial response peak time surface plot has some random fluctuations that exist due to the interaction of certain combinations of PI parameters that may influence the behaviour of the model and the numerical integration (i.e. smaller proportional and/or integral gains). Compared to the below rated wind speed scenario when the pitch angle control is not active (Fig. 9a), strength of the inertial response is much more sensitive to $K_p^{\mathrm{inner}} > 1$ (Fig. 9d) for about an order of the magnitude (10^{-3}). The only visible impact is in the initial fast transient behaviour as shown in Fig. 9c. Therefore, the dynamics of the inner loop can be neglected in DFIG inertial dynamics and they don't have an influence on the inertial response.

3.4. Impact of pitch control

Pitch control is active only at above rated wind speeds to keep the rotor from over-speeding. There are four main parameters which we have studied to see how they impact the DFIG inertial response: proportional and integral gain of the PI controller (K_p^{pitch} and K_i^{pitch}, respectively) that generates the pitch servo reference β^*, time constant of the pitch servo mechanism T_s and the pitch rate limit.

3.4.1. PI controller

K_p^{pitch} and K_i^{pitch} are varied between 80 and 300, and 0 and 30, respectively. Stronger inertial response is achieved with larger K_p^{pitch} while the K_i^{pitch} doesn't have a significant influence on the strength of the inertial response (Fig. 10a). Time at which the peak of the active power injection occurs is longer for bigger K_p^{pitch} while the K_i^{pitch} doesn't have a significant contribution (Fig. 10b). Fig. 10c shows two DFIG inertial responses for a couple of characteristic combinations of the pitch PI controller. We can conclude that the pitch PI controller parameters should be taken into account when studying virtual inertial dynamics during above rated wind speeds

3.4.2. Pitch servomechanism time constant and rate limiter

Generally, peak value of the inertial response decreases (Fig. 11a) and the peak time of the inertial response increases (Fig. 11b) for increasing the pitch servo time constant. However, this sensitivity is not significant: peak value changes are in the order of 10^{-4} and peak time changes are in the order of 10^{-2}. Therefore, pitch servo time constant for some characteristic values does not have a significant impact on the

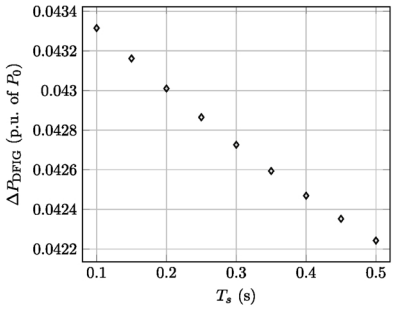

(a) DFIG power injection peak value as a function of T_s

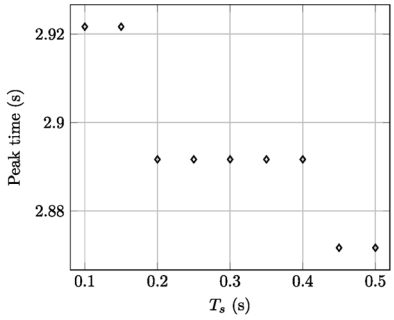

(b) DFIG power injection peak time value as a function of T_s

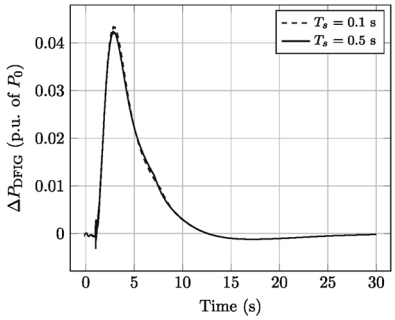

(c) DFIG power injection relative to the initial power P_0 for some characteristic combinations of T_s

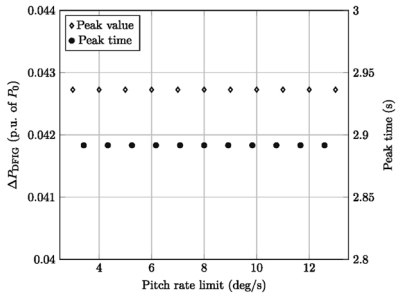

(d) DFIG power injection peak value and peak time for varying pitch rate limit

Fig. 11. Dynamic characteristics of the DFIG inertial response for different pitch servo time constant T_s.

DFIG inertial response (Fig. 11c). Pitch rate limit has been changed from ± 3°/s to ± 13°/s and it also does not influence the dynamics of the inertial response (Fig. 11d).

3.5. Impact of LSC and DC capacitor

Line-side converter keeps the DC capacitor voltage constant and controls the power factor of the LSC. Inner current control loops will be disregarded in this section since they are fast and do not influence the inertial response as shown in section 3.3.2. Varying the GSC DC loop parameters does not influence the inertial response of DFIG, as can be seen in Fig. 12a–d. Furthermore, the capacitance of the DC link capacitor does not impact the inertial response dynamics (Fig. 12e). Generally, LSC and DC link dynamics can be neglected in inertial response studies.

4. Conclusion

In this paper we have thoroughly investigated the sensitivity of virtual inertial response to various parameters of the WECS using multidimensional analysis. These parameters are: initial operating point, machine-side and line-side converter controller parameters, pitch angle control parameters and PLL parameters. The conclusions are listed below.

Impact of the wind speed on the strength of the inertial response depends on the type of machine-side converter control. For total power controlled WECS, the response is weaker with increasing wind speed, while for the speed control with inverse MPPT characteristic the response is stronger with increasing wind speed. Once the pitch control becomes active, the peak is initially slightly higher than the instance before pitch angle control activation. Then, the response also becomes weaker with increasing wind speed. Near the cut-in speed, inertial response will reduce the generator speed which will result in shifting from the MPPT curve to the quasi-constant rotor speed line. This, in turn, results in a lower peak value and peak time. The gradient of the power vs. rotor speed curve in this region has an impact on the dynamics, but detailed analysis of this region was out of the scope of this paper.

Small values of PLL PI gains will result in in more oscillatory behaviour and weak damping of the local mode. Following a disturbance, the DFIG power is momentarily reduced further aggravating the grid frequency although the actual peak value is higher. On the other hand, large gains result in strong tracking, no oscillations and smaller peak value of the inertial response. Generally, PLL dynamics can be neglected if the PLL is fast and the modes are well-damped.

Outer control loop of MSC has an impact on virtual inertial response provision. If the outer loop ihas smaller PI gains, the inertial response is stronger and peak time is shorter. This is because it will take a longer time for the weaker controller to restrain the power changes towards the set-point.

Inner loop of the MSC control, DC voltage loop and the inner loop of the LSC and the DC capacitor dynamics can be neglected in the inertial response studies since they are very fast.

Between all the parameters of the pitch control subsystem, proportional gain of the PI controller has the most significant impact on the inertial response. Larger proportional gain will results in bigger power output. Inertial response is not significantly sensitive to integral gain nor to the pitch servo time constant.

Future research may include: comparative analysis between different DFIG-based wind turbine models and control structures, virtual inertia dynamics of full converter WECS with different control structures and droop dynamics of DFIG/full-converter wind turbines.

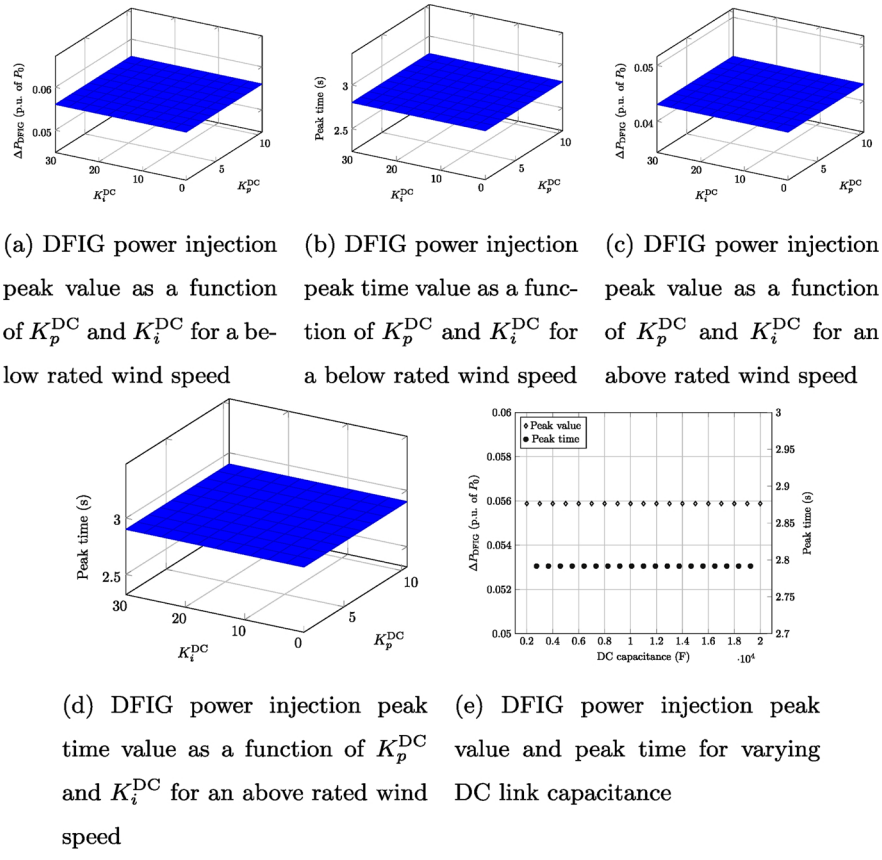

(a) DFIG power injection peak value as a function of K_p^{DC} and K_i^{DC} for a below rated wind speed

(b) DFIG power injection peak time value as a function of K_p^{DC} and K_i^{DC} for a below rated wind speed

(c) DFIG power injection peak value as a function of K_p^{DC} and K_i^{DC} for an above rated wind speed

(d) DFIG power injection peak time value as a function of K_p^{DC} and K_i^{DC} for an above rated wind speed

(e) DFIG power injection peak value and peak time for varying DC link capacitance

Fig. 12. Dynamic characteristics of the DFIG inertial response for different LSC DC voltage loop PI controller parameters.

[Test system parameters]

Wind turbine and shaft parameters: nominal/base power: 2 MVA; rotor radius: 37.5 m; gearbox ratio: 87; nominal wind speed: 12 m/s; turbine inertia constant: 4.33 s; shaft-stiffness: 0.46 p.u./el. rad.; shaft-damping: 0 p.u.

DFIG parameters: stator voltage: 690 V (line-to-line, RMS); rated apparent power: 2.28 MVA; frequency: 50 Hz; number of pole-pairs: 2; stator resistance/reactance: 0.01/0.1 p.u.; rotor resistance/reactance (referred to stator): 0.01/0.1 p.u.; magnetizing reactance: 3.5 p.u.; inertia constant: 0.6 s; DC capacitor: 10 mF.

RSC parameters: outer control loop: $Kp = 4$, $Ki = 10$; inner control loop: $Kp = 1$, $Ki = 100$.

GSC parameters: apparent power: 0.8 MVA; rated AC voltage:0.69 kV; rated DC voltage: 1.5 kV; DC voltage control loop: $Kp = 8$, $Ki = 40$; inner control loop: $Kp = 1$, $Ki = 100$.

Line-side filter: apparent power: 2 MVA; short-circuit voltage: 10%.

PLL parameters: $K_p = 50$, $K_i = 150$.

Pitch angle controller parameters: $K_p = 150$, $K_i = 25$; servo-mechanism time constant: 0.3 s; max. rate-of-change-of-pitch: ± 10°/s.

Auxilliary frequency controller parameters: $K_v = 10$; $\tau_v = 1$ s; $\tau_w = 1$; $K_d = 0$.

Synchronous generator parameters: Apparent power: 75 MVA; nominal voltage: 20 kV (line-to-line, RMS); Inertia constant: 3 s; stator resistance/reactance: 0.05/0.1 p.u.; synchronous reactance x_d/x_q: 1.5/1.5 p.u.; transient reactance x_d'/x_q': 0.256/0.3 p.u.

AVR parameters (IEEET1): default parameters in DIgSILENT PowerFactory.

Turbine-governor (TGOV1) parameters: high-pressure fraction F_H: 0.3, reheat time constant T_r: 8 s; droop: 5 %; governor time constant T_g: 0.3 s.

0.69/20 kV transformer parameters: nominal power: 100 MVA; short-circuit voltage: 10%; copper losses: 500 kW.

20/220 kV transformer parameters: nominal power: 3 MVA; LV/HV voltage ratio: 0.69/20 kV; short-circuit voltage: 10%; copper losses: 30 kW.

Overhead line parameters: rated voltage: 220 kV; rated current: 0.4 kA; resistance: 0.05 Ω/km; reactance: 0.488 Ω/km; length: 10 km.

Acknowledgements

The work of the authors is a part of the H2020 project CROSSBOW – CROSS BOrder management of variable renewable energies and storage units enabling a transnational Wholesale market (Grant No. 773430). This document has been produced with the financial assistance of the European Union. The contents of this document are the sole responsibility of authors and can under no circumstances be regarded as reflecting the position of the European Union. This work has been supported in part by the Croatian Science Foundation under the project WINDLIPS –WIND energy integration in Low Inertia Power System (grant No. HRZZ-PAR-02-2017-03).

References

[1] J. Morren, J. Pierik, S.W.H. de Haan, Inertial response of variable speed wind turbines, Electric Power Syst. Res. 76 (11) (2006) 980–987, https://doi.org/10.1016/j.epsr.2005.12.002.

[2] S. Engelken, A. Mendonca, M. Fischer, Inertial response with improved variable recovery behaviour provided by type 4 WTs, IET Renew. Power Gen. 11 (3) (2017) 195–201.

[3] M.H. Fini, M.E.H. Golshan, Determining optimal virtual inertia and frequency control parameters to preserve the frequency stability in islanded microgrids with high penetration of renewables, Electric Power Syst. Res. 154 (2018) 13–22, https://doi.org/10.1016/j.epsr.2017.08.007.

[4] M. Hwang, E. Muljadi, G. Jang, Y.C. Kang, Disturbance-adaptive short-term frequency support of a DFIG associated with the variable gain based on the ROCOF and rotor speed, IEEE Trans. Power Syst. 32 (3) (2017) 1873–1881, https://doi.org/10.1109/TPWRS.2016.2592535.

[5] F.S. Rahman, T. Kerdphol, M. Watanabe, Y. Mitani, Optimization of virtual inertia

considering system frequency protection scheme, Electric Power Syst. Res. 170 (2019) 294–302, https://doi.org/10.1016/j.epsr.2019.01.025.
[6] Y. Fu, X. Zhang, Y. Hei, H. Wang, Active participation of variable speed wind turbine in inertial and primary frequency regulations, Electric Power Syst. Res. 147 (2017) 174–184, https://doi.org/10.1016/j.epsr.2017.03.001.
[7] M. Krpan, I. Kuzle, Inertial and primary frequency response model of variable-speed wind turbines, J. Eng. 2017 (13) (2017) 844–848.
[8] S.G. Varzaneh, M. Abedi, G. Gharehpetian, A new simplified model for assessment of power variation of DFIG-based wind farm participating in frequency control system, Electric Power Syst. Res. 148 (2017) 220–229, https://doi.org/10.1016/j.epsr.2017.03.033.
[9] R.G. de Almeida, J.A.P. Lopes, Participation of doubly fed induction wind generators in system frequency regulation, IEEE Trans. Power Syst. 22 (3) (2007) 944–950.
[10] M. Abbes, M. Allagui, Participation of PMSG-based wind farms to the grid ancillary services, Electric Power Syst. Res. 136 (2016) 201–211, https://doi.org/10.1016/j.epsr.2016.02.028.
[11] T.K. Chau, S.S. Yu, T.L. Fernando, H.H.-C. Iu, M. Small, A Novel Control Strategy of DFIG Wind Turbines in Complex Power Systems for Enhancement of Primary Frequency Response and LFOD, IEEE Trans. Power Syst. 33 (2) (2018) 1811–1823, https://doi.org/10.1109/TPWRS.2017.2726160.
[12] M. Fakhari Moghaddam Arani, Y.A.-R.I. Mohamed, Dynamic droop control for wind turbines participating in primary frequency regulation in microgrids, IEEE Trans. Smart Grid 9 (6) (2018) 5742–5751, https://doi.org/10.1109/TSG.2017.2696339.
[13] H. Lee, M. Hwang, E. Muljadi, P. Sørensen, Y.C. Kang, Power-smoothing scheme of a DFIG using the adaptive gain depending on the rotor speed & frequency deviation, Energies 10 (4) (2017) 555, https://doi.org/10.3390/en10040555.
[14] M. Mehrasa, E. Pouresmaeil, A. Sepehr, B. Pournazarian, M. Marzband, J.P. Catalão, Control technique for the operation of grid-tied converters with high penetration of renewable energy resources, Electric Power Syst. Res. 166 (2019) 18–28, https://doi.org/10.1016/j.epsr.2018.09.015.
[15] Z. Wu, W. Gao, T. Gao, W. Yan, H. Zhang, S. Yan, X. Wang, State-of-the-art review on frequency response of wind power plants in power systems, J. Modern Power Syst. Clean Energy 6 (1) (2018) 1–16.
[16] M. Kayikci, J.V. Milanovic, Assessing transient response of DFIG-based wind plants-the influence of model simplifications and parameters, IEEE Trans. Power Syst. 23 (2) (2008) 545–554, https://doi.org/10.1109/TPWRS.2008.919310.
[17] M. Kayikci, J.V. Milanovic, Dynamic contribution of dfig-based wind plants to system frequency disturbances, IEEE Trans. Power Syst. 24 (2) (2009) 859–867, https://doi.org/10.1109/TPWRS.2009.2016062.
[18] M. Krpan, I. Kuzle, Introducing low-order system frequency response modelling of a future power system with high penetration of wind power plants with frequency support capabilities, IET Renew. Power Gen. 12 (8) (2018) 1453–1461 http://digital-library.theiet.org/content/journals/10.1049/iet-rpg.2017.0811.
[19] M. Krpan, I. Kuzle, Towards the new low-order system frequency response model of power systems with high penetration of variable-speed wind turbine generators, 2018 IEEE Power Energy Society General Meeting (PESGM), Portland, USA, 2018, pp. 1–5, , https://doi.org/10.1109/PESGM.2018.8586570.
[20] J. Ma, Y. Qiu, Y. Li, W. Zhang, Z. Song, J.S. Thorp, Research on the impact of DFIG virtual inertia control on power system small-signal stability considering the phase-locked loop, IEEE Trans. Power Syst. 32 (3) (2017) 2094–2105, https://doi.org/10.1109/TPWRS.2016.2594781.
[21] J. Ma, Y. Qiu, Y. Li, W. Zhang, Z. Song, J.S. Thorp, Model order reduction analysis of DFIG integration on the power system small-signal stability considering the virtual inertia control, IET Gen. Transmiss. Distrib. 11 (16) (2017) 4087–4095, https://doi.org/10.1049/iet-gtd.2017.0518.
[22] M.F. Arani, Y.A.R.I. Mohamed, Analysis and impacts of implementing droop control in DFIG-based wind turbines on microgrid/weak-grid stability, IEEE Trans. Power Syst. 30 (1) (2015) 385–396, https://doi.org/10.1109/TPWRS.2014.2321287.
[23] R. Quan, W. Pan, A low-order system frequency response model for DFIG distributed wind power generation systems based on small signal analysis, Energies 10 (5) (2017) 657–672.
[24] J. Hu, L. Sun, X. Yuan, S. Wang, Y. Chi, Modeling of type 3 wind turbines with df/dt inertia control for system frequency response study, IEEE Trans. Power Syst. 32 (4) (2017) 2799–2809, https://doi.org/10.1109/TPWRS.2016.2615631.
[25] M. Krpan, I. Kuzle, Y. Liu, Analysing frequency support from DFIG-based wind turbines-impact of parameters and initial conditions, 11th Mediterranean Conference on Power Generation, Transmission, Distribution and Energy Conversion, Cavtat, Croatia, 2018, pp. 1–7.
[26] T. Ackermann, Wind Power in Power Systems, 2nd Edition, Wiley, 2012.
[27] J.G. Slootweg, S.W.H. de Haan, H. Polinder, W.L. Kling, General model for representing variable speed wind turbines in power system dynamics simulations, IEEE Trans. Power Syst. 18 (1) (2003) 144–151, https://doi.org/10.1109/TPWRS.2002.807113.
[28] M. Krpan, I. Kuzle, Linearized model of variable speed wind turbines for studying power system frequency changes, IEEE EUROCON 2017, Ohrid, Macedonia, 2017, pp. 393–398.
[29] S.D. Rijcke, P. Tielens, B. Rawn, D.V. Hertem, J. Driesen, Trading energy yield for frequency regulation: Optimal control of kinetic energy in wind farms, IEEE Trans. Power Syst. 30 (5) (2015) 2469–2478.
[30] Z.-S. Zhang, Y.-Z. Sun, J. Lin, G.-J. Li, Coordinated frequency regulation by doubly fed induction generator-based wind power plants, IET Renew. Power Gen. 6 (1) (2012) 38–47.
[31] Z. Wang, C. Shen, F. Liu, Impact of dfig with phase lock loop dynamics on power systems small signal stability, 2014 IEEE PES General Meeting | Conference Exposition (2014) 1–5, https://doi.org/10.1109/PESGM.2014.6939310.
[32] A.D. Hansen, F. Iov, P.E. Sørensen, N.A. Cutululis, C. Jauch, F. Blaabjerg, Dynamic wind turbine models in power system simulation tool DIgSILENT, Tech. Rep. 1440 (2) (2007), https://doi.org/10.1016/j.triboint.2009.02.004 Danmarks Tekniske Universitet, Risø Nationallaboratoriet for Baeredygtig Energi.